

ORIGINAL ARTICLE

Open Access



Neural Network Robust Control Based on Computed Torque for Lower Limb Exoskeleton

Yibo Han¹, Hongtao Ma², Yapeng Wang^{3,4}, Di Shi¹, Yanggang Feng¹, Xianzhong Li¹, Yanjun Shi¹, Xilun Ding¹ and Wuxiang Zhang^{1*}

Abstract

The lower limb exoskeletons are used to assist wearers in various scenarios such as medical and industrial settings. Complex modeling errors of the exoskeleton in different application scenarios pose challenges to the robustness and stability of its control algorithm. The Radial Basis Function (RBF) neural network is used widely to compensate for modeling errors. In order to solve the problem that the current RBF neural network controllers cannot guarantee the asymptotic stability, a neural network robust control algorithm based on computed torque method is proposed in this paper, focusing on trajectory tracking. It innovatively incorporates the robust adaptive term while introducing the RBF neural network term, improving the compensation ability for modeling errors. The stability of the algorithm is proved by Lyapunov method, and the effectiveness of the robust adaptive term is verified by the simulation. Experiments wearing the exoskeleton under different walking speeds and scenarios were carried out, and the results show that the absolute value of tracking errors of the hip and knee joints of the exoskeleton are consistently less than 1.5° and 2.5°, respectively. The proposed control algorithm effectively compensates for modeling errors and exhibits high robustness.

Keywords Lower limb exoskeleton, Model compensation, RBF neural network, Computed torque method

1 Introduction

Lower limb exoskeletons, as wearable devices, have been widely used in medical [1–4], military [5, 6], industrial [7–9] and other fields. In the medical field, exoskeletons are primarily designed for patients with movement impairments. In such case, the exoskeleton usually works in conjunction with the corresponding trolley, which

provides support and guidance to ensure safety and keep balance for the wearers [10, 11]. In military and industrial fields, exoskeletons transmit the load borne by the wearer (such as backpacks or heavy tools) to the ground [12, 13], reducing fatigue and enhancing endurance and load capacity. Currently, lower limb exoskeletons are applied in different scenarios and the collaboration modes can be generally categorized into trolley-assisted mode, independent mode, and load-bearing mode.

As a nonlinear coupled system, the modeling error of the lower limb exoskeleton primarily originates from two sources. On the one hand, the dynamic model parameters cannot be accurately obtained, and on the other hand, external disturbances, especially at different application scenarios, introduce uncertainties. These factors result in existing and unknown modeling error [14]. Conventional proportional-derivative (PD) control [15],

*Correspondence:

Wuxiang Zhang
zhangwuxiang@buaa.edu.cn

¹ School of Mechanical Engineering and Automation, Beihang University, Beijing 100191, China

² Beihang Goer (Weifang) Intelligent Robot Co., Ltd., Beihang University, Weifang, China

³ Research Center of Satellite Technology, Harbin Institute of Technology, Harbin, China

⁴ Beijing Xinfeng Aerospace Equipment Co., Ltd, Beijing, China



© The Author(s) 2024. **Open Access** This article is licensed under a Creative Commons Attribution 4.0 International License, which permits use, sharing, adaptation, distribution and reproduction in any medium or format, as long as you give appropriate credit to the original author(s) and the source, provide a link to the Creative Commons licence, and indicate if changes were made. The images or other third party material in this article are included in the article's Creative Commons licence, unless indicated otherwise in a credit line to the material. If material is not included in the article's Creative Commons licence and your intended use is not permitted by statutory regulation or exceeds the permitted use, you will need to obtain permission directly from the copyright holder. To view a copy of this licence, visit <http://creativecommons.org/licenses/by/4.0/>.

sliding mode control [16], and computed torque control [17] methods cannot achieve control objectives when the modeling error is large. The complex modeling error of the exoskeleton in different application scenarios poses new challenges to the robustness and stability of its control system.

To address this issue, many researchers have proposed model compensation methods [18], among most of them combining control algorithms with neural networks [19–21]. Chen et al. [22] proposed a back stepping controller with a finite-time extended state observer to estimate and compensate lumped uncertainty. Long et al. [23] used an extended state observer-based nonlinear terminal sliding mode control to estimate and compensate for inaccuracy of model parameters and external disturbances in exoskeleton. Gao et al. [24] proposed a dual Radial Basis Function (RBF) neural network adaptive sliding mode controller to track the gait profile, compensate for frictional forces and external perturbations. Song et al. [25] proposed an adaptive fuzzy neural sliding mode control method, which approximates the uncertain term in the dynamic model through the RBF neural network to achieve precise torque output for the series elastic actuator of the exoskeleton. Neural networks have been widely used in control due to their strong learning and adaptive abilities, especially RBF neural networks, which have universal approximation capabilities that improve the robustness of control systems [19] and handle periodic disturbances. Trajectory tracking is the basic function of most lower limb exoskeletons, and this paper focuses on the research of modeling error compensation methods from the perspective of trajectory tracking control. Yin et al. [26] proposed a neural network control method based on computed torque control, which uses RBF neural network to compensate for unknown dynamic interference and complete trajectory tracking task. However, the performance of the RBF compensation controller is still determined by the upper bound of external disturbances, and large disturbances may affect tracking accuracy or even cause system unstable. Ren et al. [27] used RBF neural network to estimate exoskeleton dynamic parameters and used the gradient descent method to sequentially solve the optimal neural network parameters. Duong et al. [28] and Chen et al. [29] used RBF neural network and designed adaptive update laws to compensate for model uncertainties. Yang et al. [30] combined sliding mode control method with RBF neural network to compensate for exoskeleton modeling errors to achieve trajectory tracking. However, they can only guarantee that the error converges to a small domain and cannot ensure asymptotic stability of the system. In summary, most current model compensation methods with RBF neural network cannot make the error completely

converge, and cannot meet the robustness requirements of lower limb exoskeletons under multiple scenarios. It is of great significance to combine RBF neural network with conventional control methods and propose an improved compensation modeling error algorithm.

Addressing the high anti-interference ability and robustness requirements of lower limb exoskeletons in multiple scenarios and targeting the universal approximation ability of RBF neural networks, this paper proposes a neural network robust control algorithm based on computed torque method, focusing on the trajectory tracking control. The algorithm introduces RBF neural network compensating for uncertain parameter terms in computed torque methods. On this basis, it innovatively introduces the robust adaptive term to compensate for neural network modeling errors, overcoming the limitation of incomplete error convergence in most RBF neural network compensation methods. This ensures that the exoskeleton maintains high robustness in different usage scenarios. Experiments wearing the exoskeleton are conducted under different gait speeds and scenarios, including trolley-assisted, independent, and load-bearing modes. The results demonstrate that the lower limb exoskeleton can track the predetermined trajectories under different conditions.

The main contribution of this work can be summarized as:

(i) This paper proposes a neural network robust control algorithm based on computed torque to compensate for system modeling errors and complete trajectory tracking, which innovatively incorporates the robust adaptive term to guarantee the system asymptotically stable.

(ii) The control algorithm proposed in this paper has high robustness and has been validated in experimental scenarios under different collaborative modes. To our limited knowledge, experimental verification methods in multiple scenarios have not yet been adopted.

The rest of this paper is organized as follows. Section 2 introduces the mechanical structure and electrical system of the lower limb exoskeleton, and conducts the dynamic modeling. Section 3 proposes the neural network robust control algorithm based on computed torque and provides the stability proof using the Lyapunov method. Section 4 completes the comparative simulations, and carries out experiments on walking with exoskeleton at different gait speeds and under different collaboration modes. The results are analyzed and discussed.

2 System Description

2.1 Mechanism Design

The main driving force for human movement comes from the freedom of flexion/extension of the lower limb joints. The freedom of adduction/abduction is mainly

used to maintain balance, and the freedom of internal/external rotation is mainly used to achieve body rotation and turning during walking. Among them, the hip joint plays a crucial role in coordinating the trunk and lower limb force generation, while the knee joint bears significant pressure and consumes more energy during walking [31]. Therefore, the flexion/extension degree of freedom for the hip and knee joints are selected as active degrees of freedom for the exoskeleton. The adduction/abduction of the hip joint, and dorsiflexion/plantarflexion, internal/external rotation degrees of freedom of the ankle joint are chosen as passive degrees of freedom. The hip joint adduction/abduction is used to maintain the balance between the human and the exoskeleton, while the ankle joint internal/external rotation adapts to the wearer's turning movements.

The mechanical structure design of the lower limb exoskeleton is carried out, as shown in Figure 1. Force sensors are arranged between the binding component and the connecting component on the thigh and calf rod, as shown in Figure 1(c), to obtain the human-exoskeleton interaction forces during walking. Springs are symmetrically attached on both sides of the ankle joint to provide dorsiflexion torque, as shown in Figure 1(d). The waist crossbeam, waist link, thigh rod, and calf rod are equipped with an array of through holes that can be adjusted in length to accommodate wearers with different heights. The mechanical limits are designed at each joint of the lower limb exoskeleton to restrict the maximum range of motion for safety.

2.2 Electrical System

The hardware system is built, as shown in Figure 2(a). The main controller (Beckhoff embedded PC controller CX5130) communicates with the PC, drive modules, and sensors through the EtherCAT protocol. The hip and knee joint of exoskeleton are actuated by the robot joint module (RJSIIZ-20 and RJSIIZ-17 respectively), which integrate motors, servo drives, absolute encoders, harmonic reducers, and brakes, etc. The interaction forces are measured by four 2D force sensors (SBT673), with their analog signals transformed into digital via transmitter (SBT904D). The exoskeleton uses a 48 V rechargeable lithium battery as the power source, and is equipped with a voltage conversion module that can output 24 V voltage. In addition, a stop switch is set up for emergency braking to ensure safety for the wearer.

To improve the convenience and aesthetics of the exoskeleton, the hardware units are integrated into the control cabinet and installed at the exoskeleton waist. Corresponding shells are designed to wrap around the exoskeleton to protect the robot joint modules. The overall exoskeleton system is shown in Figure 2(b).

2.3 Lower Limb Exoskeleton Dynamic Model

The exoskeleton can be regarded as a multi-link series mechanism. Since active actuators are used at the hip and knee joints, only the thigh and calf links need to be considered when performing dynamic modeling. As a coupled system, the exoskeleton is inevitably affected by the forces of the wearer and the external environment during

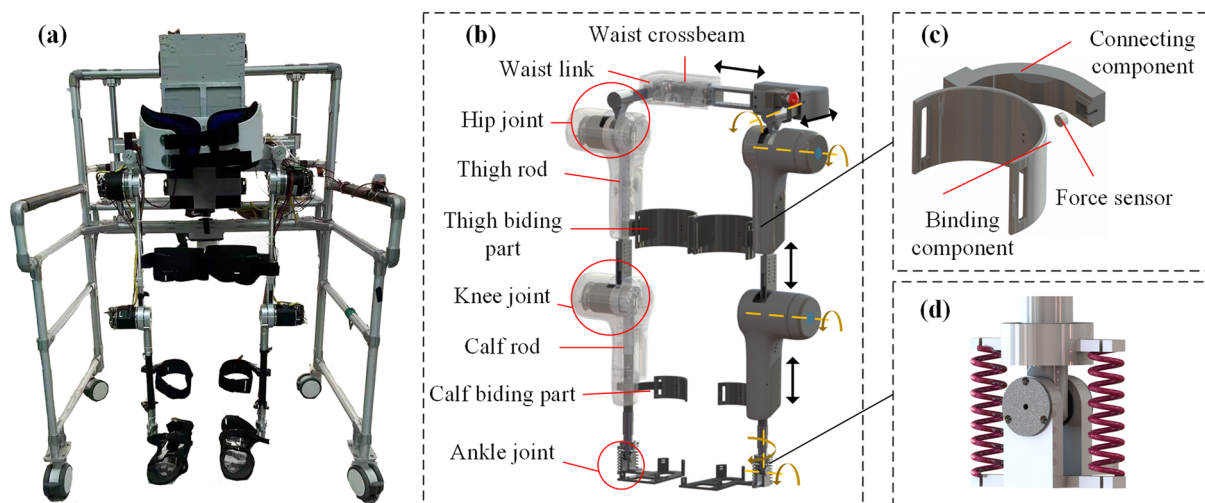


Figure 1 Structure of the applied exoskeleton: (a) Overview of the exoskeleton prototype, (b) Detailed display of the exoskeleton, (c) Force sensor arrangement, (d) The ankle joint of the exoskeleton

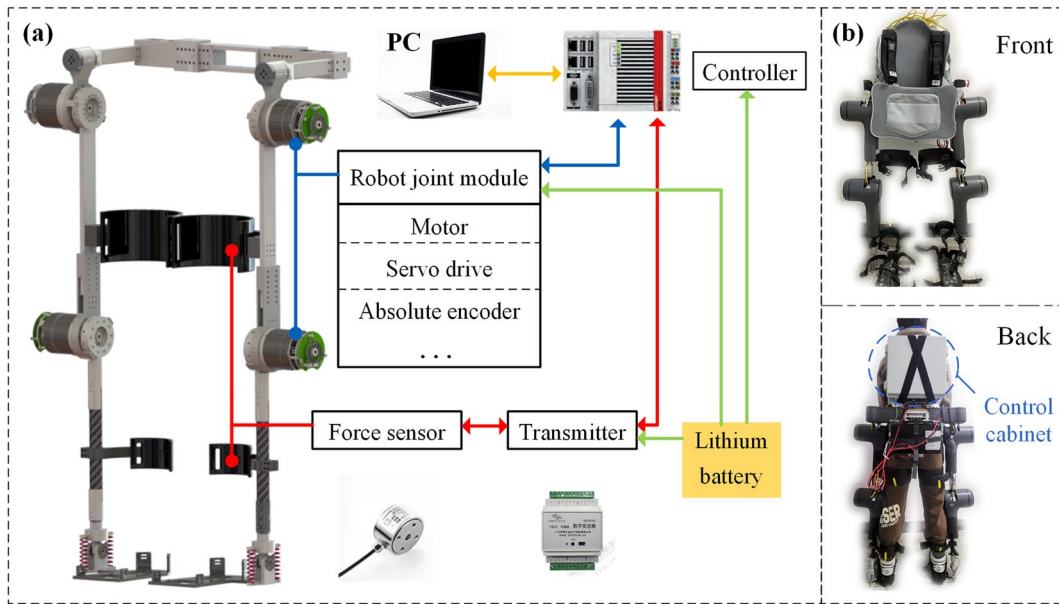


Figure 2 Overview of the exoskeleton system: (a) Hardware system, (b) Front and back view of exoskeleton system

walking. For exoskeleton that track the predetermined trajectory, these unknown disturbance forces will affect the dynamic performance of the robot and must be taken into account in the dynamic modeling.

The exoskeleton is often considered as a two-link mechanism during the swing phase of walking with the waist as the fixed frame, and as a three-link mechanism during the stance phase with the ankle joint connected to the ground through a hinge in the sagittal plane [32]. However, the dynamic model of the three-link mechanism is more complex than that of the two-link mechanism, which increases the complexity of the control algorithm accordingly. In this paper, when considering the exoskeleton in the stance phase, the ground reaction forces acting on the ankle joint are treated as a disturbance, and the robot is still regarded as a two-linkage mechanism in the sagittal plane, as shown in Figure 3, which simplifies the dynamic model but also increases the robustness requirements for the control algorithm. With Lagrangian equation, the dynamic model of the exoskeleton can be uniformly expressed as

$$M(q)\ddot{q} + C(q, \dot{q})\dot{q} + G(q) = \tau_a + F, \quad (1)$$

where $\ddot{q}, \dot{q}, q \in \mathbb{R}^2$ is the angle, angular velocity, and angular acceleration vectors at the hip and knee joints. M is the inertia matrix, C is the Coriolis and centrifugal force matrix, G is the gravity matrix. The parameters of the nominal model of the robot are shown in Eq. (2). And $\tau_a = [\tau_{a1}, \tau_{a2}]^T$ is the torque of the motor at the hip and knee joints, respectively. F is the external disturbance, which broadly include environmental forces and the

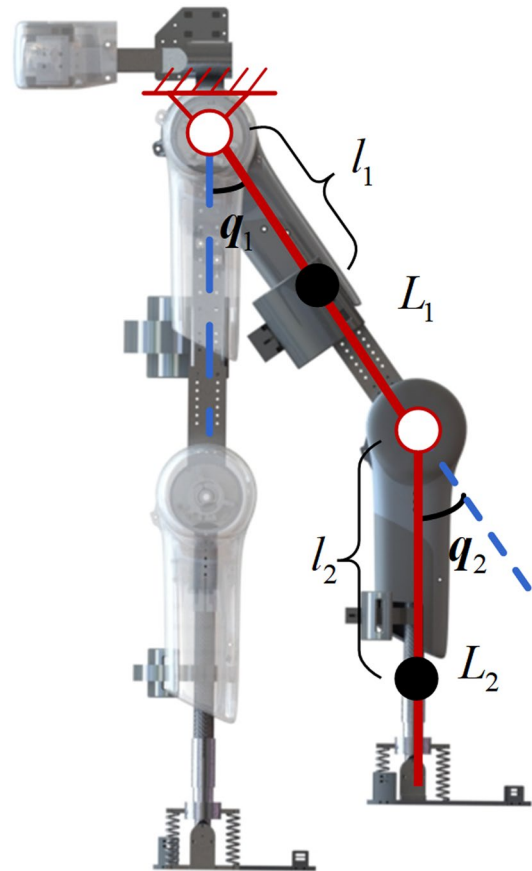


Figure 3 Two-link mechanism model

human-exoskeleton interaction torque on the exoskeleton, etc., with an unknown upper bound.

$$\begin{aligned}
 \mathbf{M} &= \begin{bmatrix} m_1 l_1^2 + m_2 L_1^2 + 2m_2 L_1 l_2 \cos q_2 + m_2 l_2^2 & -m_2 (L_1 l_2 \cos q_2 + l_2^2) \\ -m_2 (L_1 l_2 \cos q_2 + l_2^2) & m_2 l_2^2 \end{bmatrix}, \\
 \mathbf{C} &= \begin{bmatrix} -2m_2 L_1 l_2 \dot{q}_2 \sin q_2 & m_2 L_1 l_2 \dot{q}_2 \sin q_2 \\ m_2 L_1 l_2 \dot{q}_1 \sin q_2 & 0 \end{bmatrix}, \\
 \mathbf{G} &= \begin{bmatrix} (m_1 l_1 + m_2 L_1) g \sin q_1 + m_2 l_2 g \sin (q_1 - q_2) \\ -m_2 l_2 g \sin (q_1 - q_2) \end{bmatrix},
 \end{aligned} \tag{2}$$

where m_1, L_1, l_1 represents the mass, length, and length from the center of mass to the hip joint of the exoskeleton thigh rod, respectively. And m_2, L_2, l_2 represents the mass, length, and length from the center of mass to the knee joint of the exoskeleton calf rod, respectively. The parameter values are summarized in Table 1.

3 Neural Network Robust Controller Design

Tracking the predefined trajectory is the basic function of the lower limb exoskeletons. This paper focuses on the modeling error compensation method from the perspective of trajectory tracking control.

In this section, a control algorithm is proposed based on the computed torque method. It combines RBF neural networks and innovatively introduces a robust adaptive term to compensate for the uncertainties of the model and complete trajectory tracking tasks. The stability proof is performed using the Lyapunov method.

3.1 Computed Torque Controller Design

The computed torque method is a control scheme that introduces compensation in the internal control loop to linearize nonlinear systems. According to the computed torque method, combined with Eq. (1), the control law for the motor torque of the exoskeleton can generally be designed as:

$$\begin{aligned}
 \boldsymbol{\tau} &= \mathbf{M}(\mathbf{q}) [\ddot{\mathbf{q}}_d + \mathbf{k}_d(\dot{\mathbf{q}}_d - \dot{\mathbf{q}}) + \mathbf{k}_p(\mathbf{q}_d - \mathbf{q})] \\
 &\quad + \mathbf{C}(\mathbf{q}, \dot{\mathbf{q}})\dot{\mathbf{q}} + \mathbf{G}(\mathbf{q}) - \mathbf{F},
 \end{aligned} \tag{3}$$

where \mathbf{q}_d is the desired joint angle vector, and \mathbf{q} is the actual joint angle vector of the exoskeleton. $\mathbf{k}_d, \mathbf{k}_p \in \mathbb{R}^{2 \times 2}$ are the positive diagonal gain matrices.

Combining Eq. (1) and Eq. (3), we obtain

$$\ddot{\mathbf{e}} + \mathbf{k}_d \dot{\mathbf{e}} + \mathbf{k}_p \mathbf{e} = 0, \tag{4}$$

where $\ddot{\mathbf{e}} = \ddot{\mathbf{q}}_d - \ddot{\mathbf{q}}, \dot{\mathbf{e}} = \dot{\mathbf{q}}_d - \dot{\mathbf{q}}, \mathbf{e} = \mathbf{q}_d - \mathbf{q}$ represents the angular acceleration error, angular velocity error and angular error vector for each joint of the exoskeleton, respectively. From Eq. (4), it can be seen that this control law can ideally make the exoskeleton track a predetermined trajectory.

However, the computed torque method is an algorithm that relies heavily on the accuracy of the dynamic model. In reality, it is not possible to obtain accurate dynamic model parameters of the exoskeleton, but only an estimate of the inertia matrix $\hat{\mathbf{M}}(\mathbf{q})$, the Coriolis matrix $\hat{\mathbf{C}}(\mathbf{q}, \dot{\mathbf{q}})$ and the gravity matrix $\hat{\mathbf{G}}(\mathbf{q})$. The dynamic modeling error can be expressed as:

$$\Delta \mathbf{M} = (\mathbf{M} - \hat{\mathbf{M}})\ddot{\mathbf{q}} + (\mathbf{C} - \hat{\mathbf{C}})\dot{\mathbf{q}} + (\mathbf{G} - \hat{\mathbf{G}}). \tag{5}$$

In addition, in the trajectory tracking case, the exoskeleton considers human-robot interaction torque and the ground reaction forces as disturbances during the walking. However, there is a certain deviation between the observation values and the true values of interaction force sensors or foot pressure sensors. Furthermore, unknown external disturbances cannot be directly measured. Thus, the disturbance \mathbf{F} experienced by the exoskeleton is constantly changing, oscillating, and unknown during the gait cycle.

The modeling errors to be compensated for refers to the combination of the aforementioned uncertainties. Here, \mathbf{D} is used to comprehensively represent the generalized modeling error caused by the inaccurate dynamic parameters, external forces, and the wearer's forces in Eq. (6):

$$\mathbf{D} = \Delta \mathbf{M} - \mathbf{F}. \tag{6}$$

Then Eq. (3) should be rewritten as

$$\begin{aligned}
 \boldsymbol{\tau} &= \hat{\mathbf{M}}(\mathbf{q}) [\ddot{\mathbf{q}}_d + \mathbf{k}_d(\dot{\mathbf{q}}_d - \dot{\mathbf{q}}) + \mathbf{k}_p(\mathbf{q}_d - \mathbf{q})] \\
 &\quad + \hat{\mathbf{C}}(\mathbf{q}, \dot{\mathbf{q}})\dot{\mathbf{q}} + \hat{\mathbf{G}}(\mathbf{q}) + \mathbf{D}.
 \end{aligned} \tag{7}$$

Table 1 The parameter values of the nominal model

m_1 (kg)	3.2	m_2 (kg)	2.5
L_1 (m)	0.43	L_2 (m)	0.35
l_1 (m)	0.31	l_2 (m)	0.20

Combining Eq. (1) and Eq. (7), we obtain

$$\ddot{e} + k_d \dot{e} + k_p e = \hat{M}^{-1} (D - \hat{D}), \tag{8}$$

where \hat{D} is an estimate of the modeling error. From Eq. (8), it can be seen that the stability of the system depends on the ability to estimate D .

3.2 RBF Neural Network Robust Controller Design

The RBF neural network is a three-layer feedforward network that can be widely used for function approximation and pattern classification. Compared to other types of artificial neural networks, the RBF neural network has characteristics of a simple structure, fast learning speed, excellent approximation and generalization capability. In this paper, the RBF neural network's universal approximation capability is utilized to approximate and compensate for the modeling error in Eq. (8), as shown in Eq. (9). The hidden layer adopts seven nodes.

$$[\hat{M}^{-1} D]_i = W_i \varphi(X_i), \quad i = 1, 2, \tag{9}$$

where $W_i \in \mathbb{R}^7$ is the weight matrix of the RBF neural network and $\varphi(X_i)$ is the Gaussian basis function matrix. In this paper, $i=1$ corresponds to the hip joint variable and $i=2$ corresponds to the knee joint variable of the exoskeleton. In Eq. (9)

$$\begin{aligned} X_i &= \begin{bmatrix} e_i \\ \dot{e}_i \end{bmatrix}, \\ \varphi_{ij} &= \exp(-\|X_i - c_j\|^2 / \sigma_i^2), \quad j = 1, 2, \dots, 7, \\ \varphi(X_i) &= [\varphi_{i1} \varphi_{i2} \dots \varphi_{i7}]^T, \end{aligned} \tag{10}$$

where $c_j \in \mathbb{R}^2$ is the center vector of the Gaussian basis function, and σ_i is the width of the Gaussian basis function.

Denote the optimal RBF neural network weights as W_i^* , then the theoretical deviation between the optimal RBF neural network and the modeling error to be approximated can be expressed as

$$\delta_i = (W_i - W_i^*) \varphi(X_i). \tag{11}$$

It has been proven that $\delta \in \mathbb{R}^2$ is bounded [33, 34], and $\delta_0 = \sup \|\delta\|$, where $\sup \|\cdot\|$ denotes the upper bound of the variable.

Due to the existence of modeling errors in neural networks, most existing model compensation algorithms cannot converge error completely. To further improve the robustness of the control algorithm, it is necessary to compensate for the modelling error of the neural network and add the robust adaptive term to its control law. The motor torque control law can be designed as

$$\begin{aligned} \tau = & \hat{M}(q) [\ddot{q}_d + k_d(\dot{q}_d - \dot{q}) + k_p(q_d - q)] \\ & + \hat{C}(q, \dot{q}) \dot{q} + \hat{G}(q) + \hat{M}(q)H + h, \end{aligned} \tag{12}$$

where $H_i = \hat{W}_i \varphi(X_i)$, and $H \in \mathbb{R}^2$. $\hat{W}_i \in \mathbb{R}^7$ is the estimate of the RBF neural network weights, and $h \in \mathbb{R}^2$ represents the added robust term. These two parameters are to be solved for, and their exact representation and derivation process will be discussed later. By combining Eq. (1), Eq. (8), Eq. (9), Eq. (11) and Eq. (12), we obtain

$$\ddot{e}_i + k_{di} \dot{e}_i + k_{pi} e_i = (W_i^* - \hat{W}_i) \varphi(X_i) + \delta_i - [\hat{M}^{-1} h]_i. \tag{13}$$

Eq. (13) can be written in the form of a state space equation as

$$\dot{X}_i = A_i X_i + B[(W_i^* - \hat{W}_i) \varphi(X_i) + \delta_i - (\hat{M}^{-1} h)_i], \tag{14}$$

where

$$A_i = \begin{bmatrix} 0 & 1 \\ -k_{pi} & -k_{di} \end{bmatrix}, \quad B = \begin{bmatrix} 0 \\ 1 \end{bmatrix}. \tag{15}$$

There exists matrix $P \in \mathbb{R}^{2 \times 2}$ satisfying the Lyapunov equation $PA_i + A_i^T P = -Q \cdot Q$ is a positive definite matrix.

The introduced robustness term h is defined as follows:

$$\begin{cases} \zeta_i = \sup \|(W_i - \hat{W}_i) \varphi(X_i)\|, \\ \hat{\zeta}_i = |X_i^T P B|, \\ (\hat{M}^{-1} h)_i = \hat{\zeta}_i \text{sgn}(X_i^T P B), \end{cases} \tag{16}$$

where $\zeta \in \mathbb{R}^2$ is the upper bound on the absolute value of the deviation between the modeling error to be approximated and the actual estimated value of the RBF neural network. $\hat{\zeta}$ is the estimate of this deviation. The meaning of $\text{sgn}(\cdot)$ is shown in Eq. (17):

$$\text{sgn}(\Sigma) = \begin{cases} 1 & \text{for } \Sigma > 0, \\ 0 & \text{for } \Sigma = 0, \\ -1 & \text{for } \Sigma < 0. \end{cases} \tag{17}$$

The RBF neural network weight adaptive law is designed as follows:

$$\dot{\hat{W}}_i = [\varphi(X_i) X_i^T P B]^T. \tag{18}$$

Combining Eq. (16), and Eq. (18), the motor torque control law can be obtained in Eq. (12).

3.3 Stability Analysis

The control algorithm can ensure the system ultimately asymptotically stable. The stability proof is given below.

Define the first Lyapunov function as

$$V_1 = \frac{1}{2} X_i^T P X_i. \tag{19}$$

The first derivative of Lyapunov function shown in Eq. (19) is obtained as follows:

$$\dot{V}_1 = \frac{1}{2} (X_i^T P \dot{X}_i + \dot{X}_i^T P X_i). \tag{20}$$

Further, combining Eq. (14), we obtain:

$$\dot{V}_1 = -\frac{1}{2} X_i^T Q X_i + X_i^T P B [(W_i^* - \hat{W}_i) \varphi(X_i) + \delta_i - (\hat{M}^{-1} h)_i]. \tag{21}$$

Define the second Lyapunov function as

$$V_2 = \frac{1}{2} (W_i^* - \hat{W}_i) (W_i^* - \hat{W}_i)^T. \tag{22}$$

Combining Eq. (18) and Eq. (21), we obtain:

$$\begin{aligned} \dot{V}_1 + \dot{V}_2 &= -\frac{1}{2} X_i^T Q X_i + X_i^T P B [(W_i^* - \hat{W}_i) \varphi(X_i) \\ &\quad + \delta_i - (\hat{M}^{-1} h)_i] - (W_i^* - \hat{W}_i) \dot{\hat{W}} \\ &= -\frac{1}{2} X_i^T Q X_i + X_i^T P B [\delta_i - (\hat{M}^{-1} h)_i]. \end{aligned} \tag{23}$$

Define the third Lyapunov function as

$$V_3 = \frac{1}{2} (\zeta_i - \hat{\zeta}_i)^T (\zeta_i - \hat{\zeta}_i). \tag{24}$$

Combining Eq. (23) and Eq. (24), we obtain:

$$\begin{aligned} \dot{V}_1 + \dot{V}_2 + \dot{V}_3 &= -\frac{1}{2} X_i^T Q X_i + X_i^T P B [\delta_i - (\hat{M}^{-1} h)_i] + |X_i^T P B| (\hat{\zeta}_i - \zeta_i) \\ &= -\frac{1}{2} X_i^T Q X_i + X_i^T P B [\delta_i - \hat{\zeta}_i \text{sgn}(X_i^T P B)] + |X_i^T P B| (\hat{\zeta}_i - \zeta_i) \\ &= -\frac{1}{2} X_i^T Q X_i + X_i^T P B \delta_i - |X_i^T P B| \zeta_i \\ &\leq -\frac{1}{2} X_i^T Q X_i + |X_i^T P B| (|\delta_i| - \zeta_i). \end{aligned} \tag{25}$$

In Eq. (25), ζ is an upper bound on the absolute value of the deviation from the true value when using the actual estimated RBF neural network parameters, and δ is the deviation from the true value when using the optimal RBF neural network parameters, for which the relation $|\delta_i| \leq \zeta_i$ exists. Therefore, Eq. (26) can be obtained:

$$\dot{V} = \dot{V}_1 + \dot{V}_2 + \dot{V}_3 \leq 0. \tag{26}$$

The Lyapunov criterion proves that the algorithm proposed in this section can ensure the asymptotic stability of the control system, and the error can converge completely. The control diagram is shown in Figure 4.

4 Experiment and Discussion

4.1 Simulation and Results

To preliminarily evaluate the proposed control method, especially the effectiveness of the robust adaptive term, this section conducted the simulation using the Simulink in Matlab. Firstly, the dynamics parameters of the lower limb exoskeleton were calculated through SolidWorks software, which serves as the nominal parameters in the simulation. The actual estimated dynamic parameters were chosen as $\hat{M} = 0.3M$, $\hat{C} = 0.3C$, $\hat{G} = 0.3G$, and the external disturbance D was set as a constant. The desired trajectory was obtained by fitting human gait data from CGA [35], and the gait cycle was set as 3.0 s.

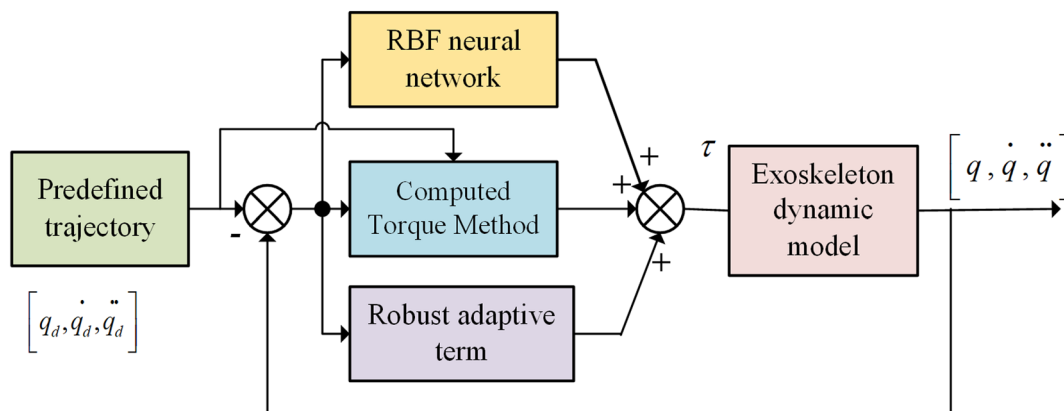


Figure 4 The control diagram

The conventional computed torque control law (CT), the neural network control law without the robustness adaptive term (CT+RBF), and the neural network robust control law with the robustness adaptive term (CT+RBF+ Robust term) were employed in the simulation, respectively. The control parameters are summarized in Table 2. With the same gains chosen, these control laws aimed to achieve trajectory tracking of the hip and knee joints of the lower limb exoskeleton in the presence of modeling errors. Among them, the neural network control law only used RBF neural network to compensate for the modeling errors, and this setting was to further evaluate the role of the robust adaptive term proposed in this paper. The simulation results with different control laws are shown in Figure 5.

The simulation results show that with the computed torque control law (CT), the neural network control law without the robustness adaptive term (CT+RBF), and the neural network robust control law with the robustness adaptive term (CT+RBF+ Robust term), the root mean square values of hip joint tracking errors are 3.62° , 0.59° , and 0.23° respectively. And the root mean square values of knee joint tracking errors are 14.73° , 1.23° , and 0.57° respectively. By comparing the simulation results, it is found that with the same gains chosen, the conventional computed torque law cannot achieve tracking the desired trajectories due to the presence of modeling errors. On the other hand, the other two laws are capable of tracking the desired trajectories, indicating that the RBF neural network plays a role in compensating for modeling errors. Comparatively, the neural network robust control law proposed in this paper demonstrates the best performance, with lower amplitude and mean values of tracking errors in hip and knee joint motions. This implies that the introduced robust term further compensates for the modeling errors. The output torques of the two algorithms are similar.

The simulation results show that the tracking error of the system can be controlled within a certain range by using the proposed control method to compensate for the uncertainty of the model. The robust adaptive

term, in particular, compensates for modeling errors and improve control performance.

4.2 Experimental Validation

Experiments on walking with the exoskeleton under different walking gait speeds and collaboration modes were conducted to evaluate the proposed control method. In the experiments with different collaboration modes including trolley-assisted mode, independent mode, and load-bearing mode, the dynamics of the exoskeleton and the external disturbances under different scenarios are different, which further verifies the high robustness of the control algorithm in this paper.

4.2.1 Experimental Protocol

Based on the experimental platform, experiments under different walking gait speeds and collaboration modes were conducted to evaluate the control algorithm's robustness and anti-disturbance capability, verifying its ability to maintain good trajectory tracking performance under different external disturbances. The participant is a healthy male with a height of 180 cm and a weight of 75 kg.

The participant provided written informed consent, and the study procedures were conducted in accordance with the Declaration of Helsinki. This research was approved by the Beihang University Biological and Medical Ethics Committee (protocol code BM20220209). During the experiment, the participant's lower limbs were driven by the robot. The predetermined gait trajectory was obtained by fitting the human CGA gait data.

In the experiment of human-robot walking at different speeds, the gait cycles were set to 3 s, 3.5 s, and 4 s, respectively. In the experiments under different scenarios, the exoskeleton was in different collaboration mode including trolley-assisted mode, independent mode, and load-bearing mode, with the gait cycle set to 3.0 s. Different experimental conditions are shown in Figure 6. Among them, when in the trolley-assisted mode, the trolley balances the weight of the exoskeleton and provides auxiliary support and protection for the wearer. When in the exoskeleton-independent mode, the weight of the

Table 2 The control parameters in the simulation

Parameter	Description	Value
k_p	Proportional gain matrix	$diag\{900, 900\}$
k_d	Derivative gain matrix	$diag\{200, 200\}$
c	Center vector of the Gaussian basis function	$\begin{bmatrix} -1.5 & -1 & -0.5 & 0 & 0.5 & 1.0 & 1.5 \\ -1.5 & -1 & -0.5 & 0 & 0.5 & 1.0 & 1.5 \end{bmatrix}$
σ	Width of the Gaussian basis function	$[0.8, 0.8]$
Q	Positive definite matrix in the Lyapunov equation	$diag\{3600, 1600\}$

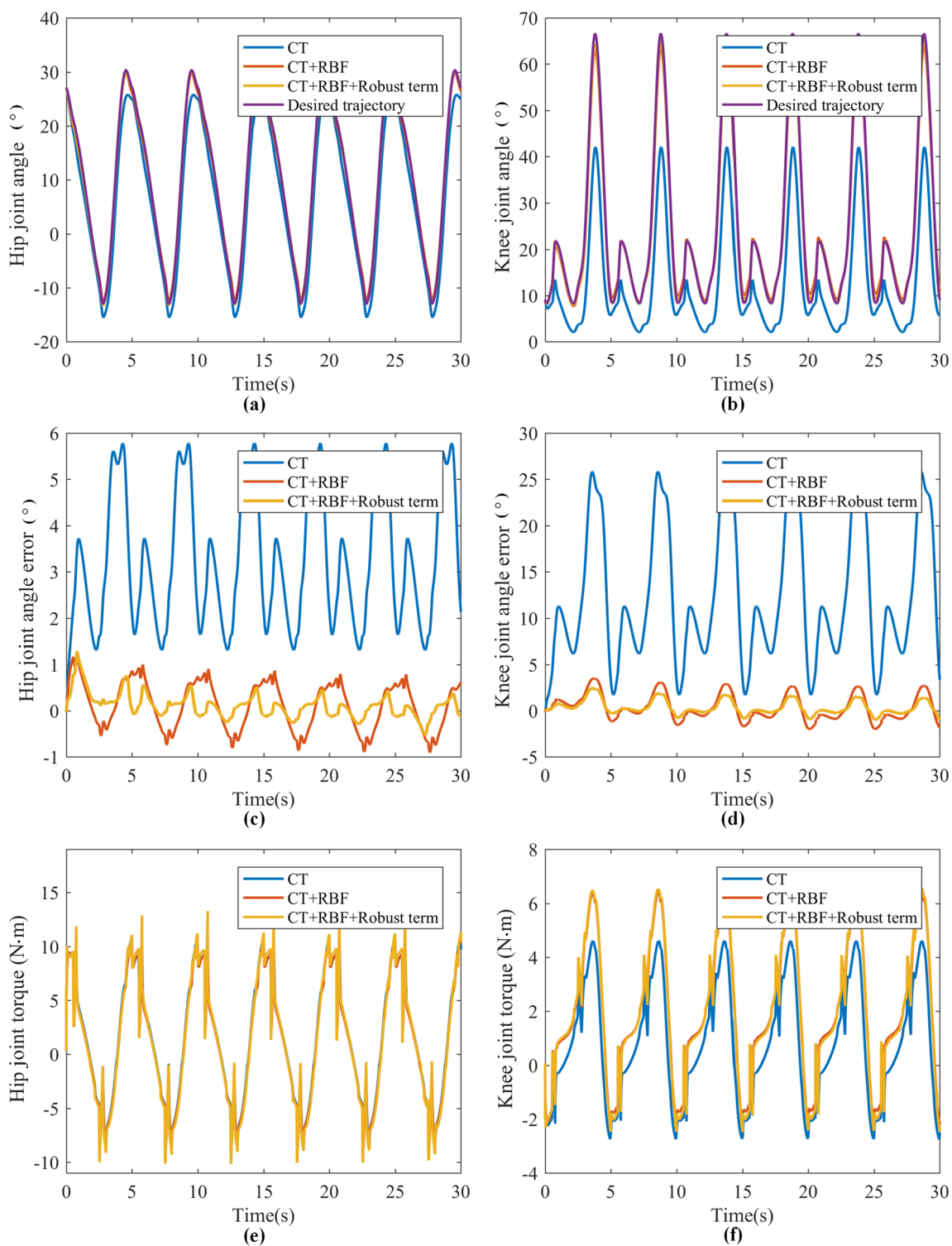


Figure 5 Simulation results: (a) Trajectory of the hip joint, (b) Trajectory of the knee joint, (c) Tracking error of the hip joint, (d) Tracking error of the knee joint, (e) Motor torque of the hip joint, (f) Motor torque of the knee joint

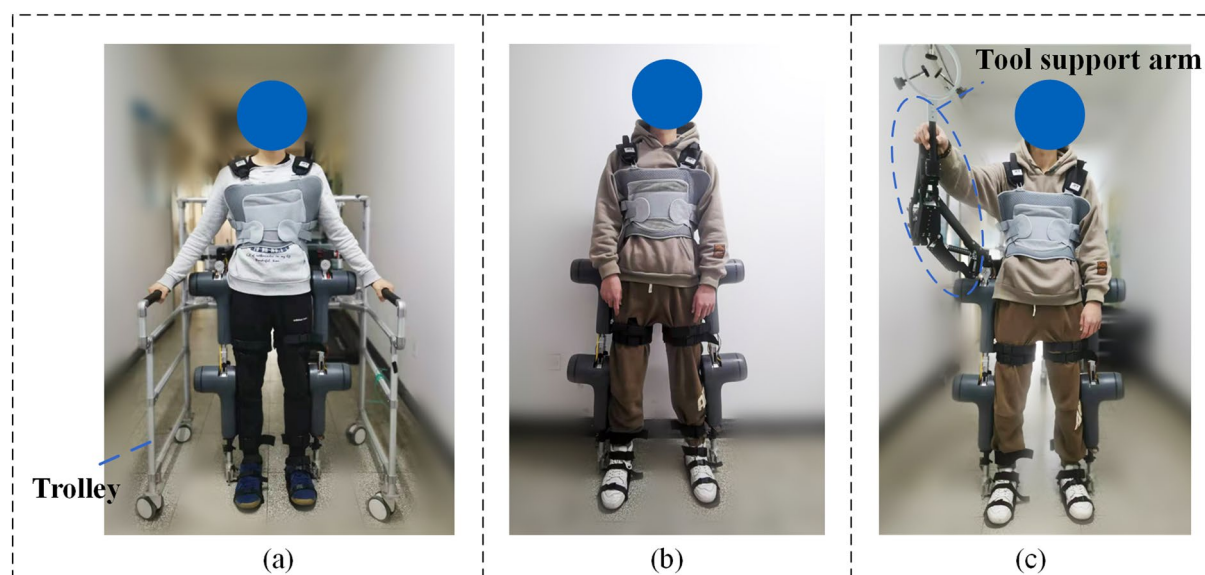


Figure 6 The experiments under different scenarios and collaboration modes: (a) Trolley-assisted, (b) Independent, (c) Load-bearing

exoskeleton is transmitted to the ground during the supporting phase, and the wearer maintains balance on their own. When in the exoskeleton-load bearing mode, the exoskeleton is equipped with a tool support arm, which can be used to assist the wearer in supporting and operating tools. The weight of the support arm is 3.0 kg and the maximum extension length is about 1.0 m.

4.2.2 Experimental Results

In the experiments with different walking gait speeds, the tracking errors between the desired and actual trajectory of the exoskeleton, joint torque, and interaction force are shown in Figure 7. The human-robot interaction force is considered a disturbance in the control algorithm and can also indicate the coordination between the wearer and the exoskeleton during walking.

When the gait cycle is 4.0 s, 3.5 s, and 3.0 s, respectively, the corresponding maximum hip joint tracking error is about 1.5°, which is lower than 3.7% of the joint motion amplitude, and the root mean square (RMS) values are 0.55°, 0.63°, and 0.74°. The maximum knee joint tracking error is about 2.2°, 2.1°, and 2.5°, respectively, which is lower than 4.5% of the joint motion amplitude, and the RMS values are 1.2°, 1.3°, and 1.5°. The RMS values of the hip joint motor output torque are 17.6 N·m, 22.9 N·m, and 27.7 N·m, respectively, and the RMS values of the knee joint motor output torque are 19.1 N·m, 14.1 N·m, and 17.4 N·m, respectively. The RMS values of the human-exoskeleton interaction force at the thigh are 5.7 N, 7.4 N, and 8.3 N, respectively, and the RMS values of the human-exoskeleton interaction force at the calf are 6.7 N, 7.1 N, and 6.2 N, respectively. Overall, under

different walking gait speeds, the lower limb exoskeleton can follow to the predetermined trajectory. In addition, the weight W of RBF neural networks were recorded as shown in Figure 8. The results show that the weight fluctuate and converge around a certain value at different walking gait speeds.

In the experiments with different collaboration modes, the tracking errors between the desired and actual trajectory of the exoskeleton, joint torque, and interaction force are shown in Figure 9.

Under different conditions of trolley-assisted, independent, and load-bearing collaboration modes, the maximum hip joint tracking errors are 1.2°, 1.5°, and 1.5° respectively, which are below 3.7% of the joint motion amplitude. The RMS values are 0.53°, 0.69°, and 0.79° respectively. The maximum knee joint tracking errors are 2°, 2.3°, and 2.5° respectively, which are below 4.5% of the joint motion amplitude. The RMS values are 1.2°, 1.5°, and 1.5° respectively. The RMS values of hip joint motor output torque are 18 N·m, 25 N·m, and 30 N·m, and the RMS values of knee joint motor output torque are 16 N·m, 18 N·m, and 22 N·m. The RMS values of human-robot interaction force at the thigh are 2.1 N, 6.3 N, and 6.1 N, and the RMS values of human-robot interaction force at the calf are 7.1 N, 4.7 N, and 4.7 N. In addition, the weight W of RBF neural networks were recorded as shown in Figure 10. The results show that the weight fluctuate and converge around a certain value with different collaboration modes.

The experimental results are summarized in Tables 3 and 4.

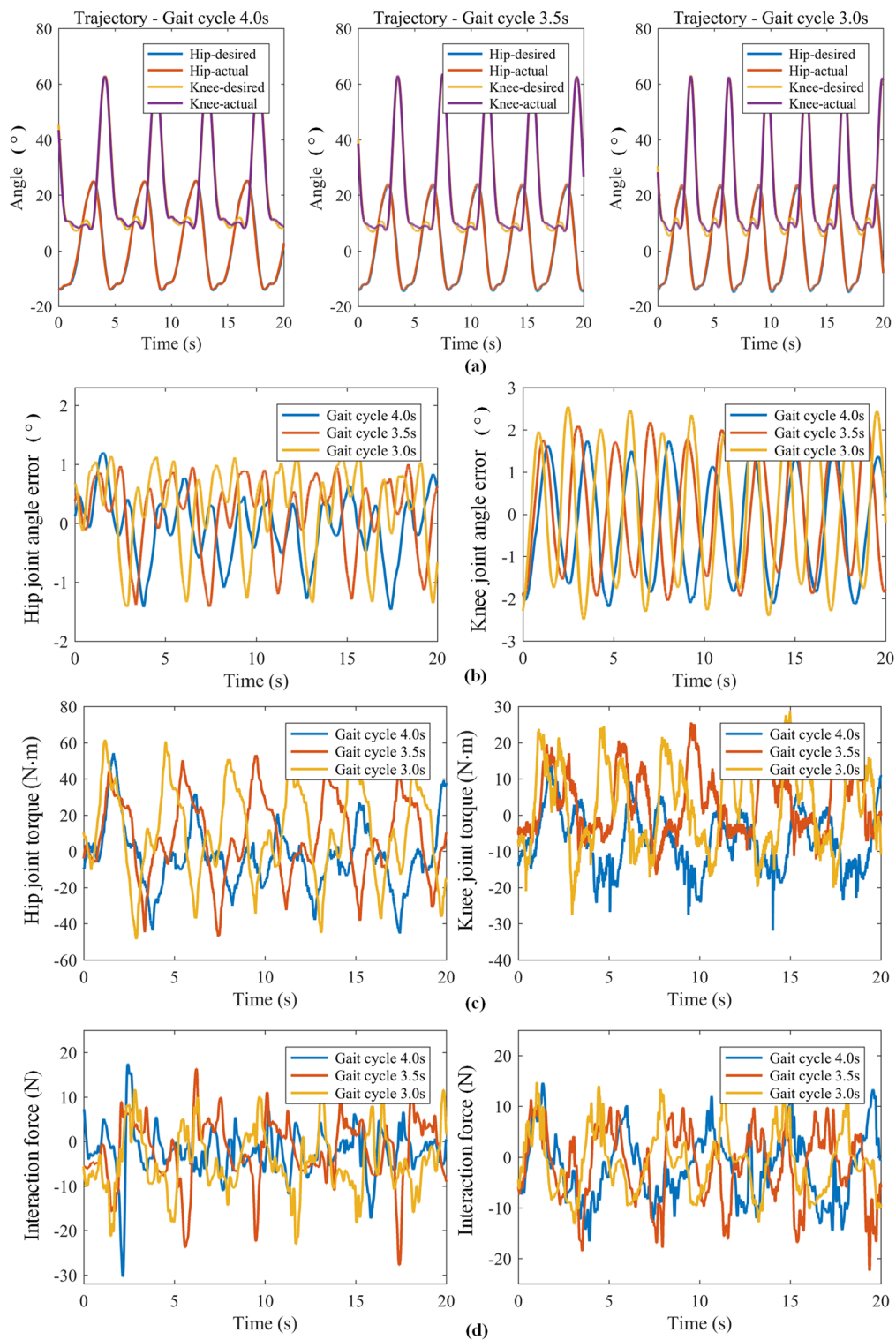


Figure 7 Experimental results with different walking gait cycles: **(a)** Trajectory of the hip joint and knee joint, **(b)** Tracking error of the hip joint and knee joint, **(c)** Motor torque of the hip joint and knee joint, **(d)** Interaction force at the thigh and the calf

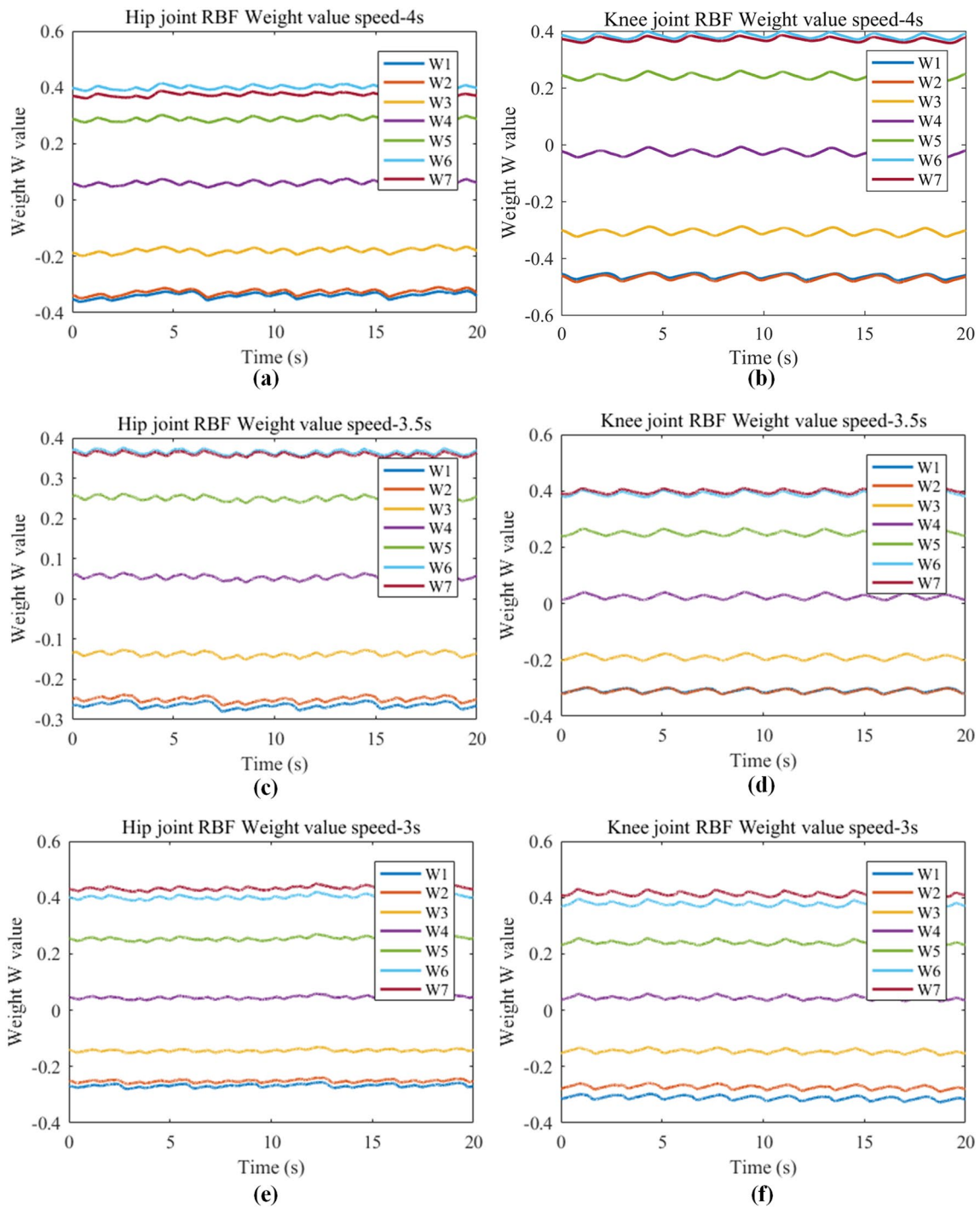


Figure 8 The weight W of RBF neural networks with different walking gait cycles

4.3 Discussion

In the simulation, the conventional computed torque control law, the neural network control law without and with the robustness adaptive term were employed to track the hip and knee joint motions of the lower limb

exoskeleton in the presence of modeling errors, respectively. The results indicate that the neural network robust control law proposed in this paper demonstrates the best performance, which means that the algorithm

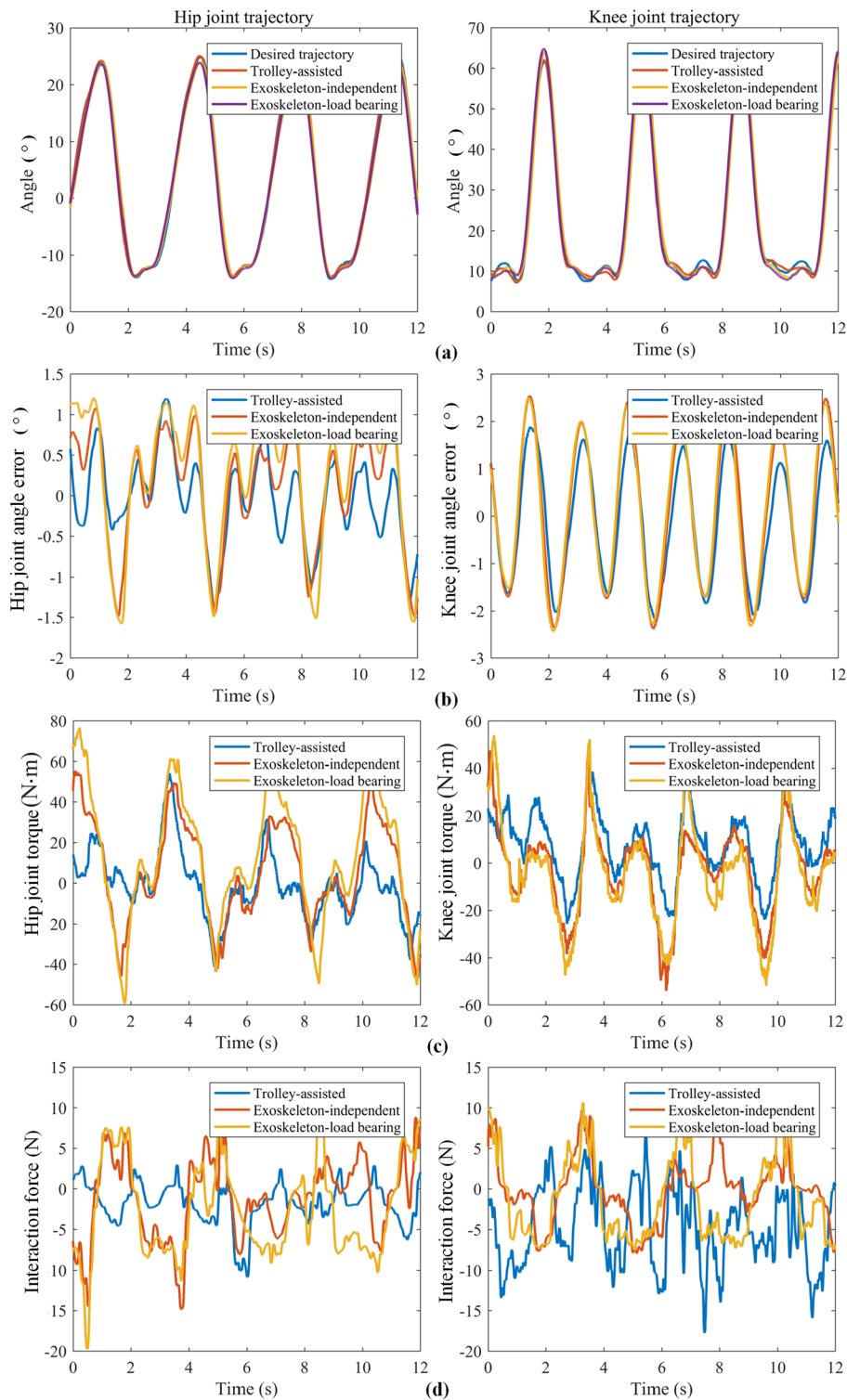


Figure 9 Experimental results with different collaboration modes: (a) Trajectory of the hip joint and knee joint, (b) Tracking error of the hip joint and knee joint, (c) Motor torque of the hip joint and knee joint, (d) Interaction force at the thigh and the calf

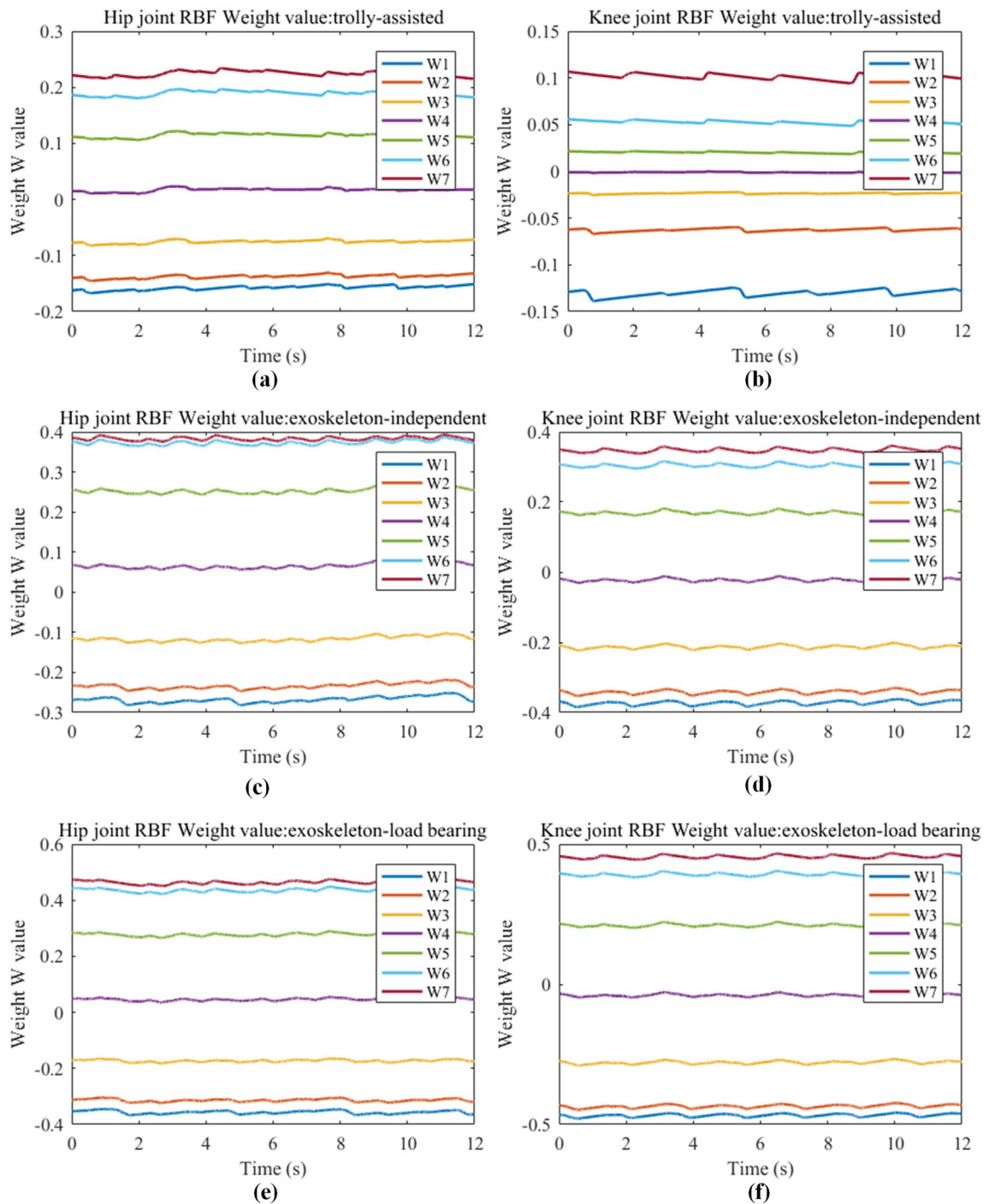


Figure 10 The weight W of RBF neural network with different collaboration modes

in this paper improves the compensation of the modeling errors compared to the traditional algorithm.

In the experiments with different walking gait speeds, the tracking errors of hip joint and knee joint remain within 3.7%, 4.3% of the joint movement amplitude respectively at different speeds. As for the output torque

of the motor, the RMS value of the hip joint motor torque slightly increases with the increase of gait frequency, since the shorter gait cycle requires the lower limb exoskeleton to respond faster.

However, the peak value of knee joint motor torque exceeds the other two gait cycles when the gait cycle is

Table 3 Summary of results with different walking gait cycles

Condition		Different walking gait cycles		
		Gait cycle 4.0 s	Gait cycle 3.5 s	Gait cycle 3.0 s
Tracking error (RMS) (°)	Hip	0.55	0.63	0.74
	Knee	1.2	1.3	1.5
Torque (RMS) (N·m)	Hip	17.6	22.9	27.7
	Knee	19.1	14.1	17.4
Interaction force (RMS) (N)	Thigh	5.7	7.4	8.3
	Calf	6.7	7.1	6.2

Table 4 Summary of results with different collaboration modes

Condition		Different collaboration modes		
		Trolley-assisted	Independent	Load-bearing
Tracking error (RMS) (°)	Hip	0.53	0.69	0.79
	Knee	1.2	1.5	1.5
Torque (RMS) (N·m)	Hip	18	25	30
	Knee	16	18	22
Interaction force (RMS) (N)	Thigh	2.1	6.3	6.1
	Calf	7.1	4.7	4.7

4.0 s. It is preliminarily believed that the 4.0 s gait cycle appears to be slow for the healthy male, and there may be a phenomenon where the intention of human calf movement is faster than that of the robot, leading to an increase in peak torque.

The tracking errors of hip joint and knee joint remain within 3.7%, 4.5% of the joint motion amplitude respectively, under trolley-assisted, independent, and load-bearing collaboration modes. For the motor output torque, the RMS values of hip and knee joint motor torque increase in the corresponding order. Since the assisted trolley can support part of the exoskeleton weight and load during the walking, these three different modes can be considered that external disturbances are increasing in sequence, resulting in an increase in motor torque. However, under the trolley-assisted mode, the amplitude of the knee joint motor torque is approximately or even greater than the motor torque under the other two modes sometimes, and similar result has also occurred in the human-exoskeleton interaction force at the calf. It is preliminarily believed that this is caused by the incongruity between the wearer and the trolley. During the walking, the wearer's waist center of gravity may fluctuate up and down, and the trolley restricts this degree of freedom (although the trolley in this paper considered this factor and incorporated a spring mechanism in the

waist, the spring with high stiffness still imposed restrictions on the wearer), which leads to discoordination between the wearer and the trolley-assisted exoskeleton, resulting in an increase in peak torque at the knee joint and human-robot interaction force at the calf.

Overall, under different usage scenarios, especially when adding a load (tool support arm), the lower limb exoskeleton can still track the desired trajectory. The control algorithm in this paper can effectively compensate for complex modeling errors and has high anti-interference capability and robustness.

5 Conclusions

Aiming to improve the model compensation capability and focusing on trajectory tracking control, a robust control algorithm based on computed torque and RBF neural networks is proposed. By introducing RBF neural network terms and robust terms, uncertain modeling errors are compensated, and the trajectory tracking ability of lower limb exoskeleton is improved. The experimental results show that in the experiments with different gait speeds and different application scenarios, the joint tracking error is always within 4.5% of the joint motion amplitude. The control algorithm can compensate for modeling errors, and has good tracking accuracy,

anti-interference ability and robustness. Currently, only the position tracking control has been analyzed and validated in this paper, which can be extended to other control methods in the future research.

Acknowledgements

The authors sincerely thank Mr. Yixin Shao of Beihang University for their critical discussion and reading during manuscript preparation.

Authors' contributions

XD, WZ and DS were in charge of the whole trial; YH wrote the manuscript; YF, YW and HM assisted with structure and language of the manuscript. YS and XL assisted in conducting experiments. All authors read and approved the final manuscript.

Funding

Supported by National Key R&D Program of China (Grant No. 2022YFB4701200) and National Natural Science Foundation of China (NSFC) (Grant Nos. T2121003, 52205004).

Declarations

Competing Interests

The authors declare no competing financial interests.

Received: 26 August 2023 Revised: 5 November 2023 Accepted: 27 March 2024

Published online: 25 April 2024

References

- [1] D Shi, W Zhang, W Zhang, et al. A review on lower limb rehabilitation exoskeleton robots. *Chinese Journal of Mechanical Engineering*, 2019, 32: 74.
- [2] A Plaza, M Hernandez, G Puyuelo, et al. Lower-limb medical and rehabilitation exoskeletons: A review of the current designs. *IEEE Reviews in Biomedical Engineering*, 2023, 16: 278-291.
- [3] C Siviyy, L M Baker, B T Quinlivan, et al. Opportunities and challenges in the development of exoskeletons for locomotor assistance. *Nature Biomedical Engineering*, 2022, 7(4): 465-472.
- [4] A J Young, D P Ferris. State of the art and future directions for lower limb robotic exoskeletons. *IEEE Transactions on Neural Systems and Rehabilitation Engineering*, 2017, 25(2): 171-182.
- [5] K L Mudie, A C Boynton, T Karakolis, et al. Consensus paper on testing and evaluation of military exoskeletons for the dismounted combatant. *Journal of Science and Medicine in Sport*, 2018, 21(11): 1154-1161.
- [6] D J Hyun, H Park, T Ha, et al. Biomechanical design of an agile, electricity-powered lower-limb exoskeleton for weight-bearing assistance. *Robotics and Autonomous Systems*, 2017, 95: 181-195.
- [7] G Ashta, S Finco, D Battini, et al. Passive exoskeletons to enhance workforce sustainability: Literature review and future research agenda. *Sustainability*, 2023, 15(9): 7339.
- [8] A Baldassarre, L G Lulli, F Cavallo, et al. Industrial exoskeletons from bench to field: Human-machine interface and user experience in occupational settings and tasks. *Frontiers in Public Health*, 2022, 10: 4375.
- [9] M P De Looze, T Bosch, F Krause, et al. Exoskeletons for industrial application and their potential effects on physical work load. *Ergonomics*, 2016, 59(5): 671-681.
- [10] S K Banala, S H Kim, S K Agrawal, et al. Robot assisted gait training with active leg exoskeleton (alex). *IEEE Transactions on Neural Systems and Rehabilitation Engineering*, 2009, 17(1): 2-8.
- [11] J Meuleman, E Van Asseldonk, G Van Oort, et al. Lopes ii-design and evaluation of an admittance controlled gait training robot with shadow-leg approach. *IEEE Transactions on Neural Systems and Rehabilitation Engineering*, 2016, 24(3): 352-363.
- [12] W J Cao, C J Chen, D S Wang, et al. A lower limb exoskeleton with rigid and soft structure for loaded walking assistance. *IEEE Robotics and Automation Letters*, 2022, 7(1): 454-461.
- [13] J J Y Liang, Q H Zhang, Y Liu, et al. A review of the design of load-carrying exoskeletons. *Science China-Technological Sciences*, 2022, 65(9): 2051-2067.
- [14] J J Sun, J Wang, P Yang, et al. Model-free prescribed performance fixed-time control for wearable exoskeletons. *Applied Mathematical Modelling*, 2021, 90: 61-77.
- [15] S Maggioni, A Melendez-Calderon, E Van Asseldonk, et al. Robot-aided assessment of lower extremity functions: A review. *Journal of Neuroengineering and Rehabilitation*, 2016, 13: 1-25.
- [16] S Hussain, S Q Xie, P K Jamwal. Robust nonlinear control of an intrinsically compliant robotic gait training orthosis. *IEEE Transactions on Systems Man Cybernetics-Systems*, 2013, 43(3): 655-665.
- [17] P K Jamwal, S Q Xie, S Hussain, et al. An adaptive wearable parallel robot for the treatment of ankle injuries. *IEEE-ASME Transactions on Mechatronics*, 2014, 19(1): 64-75.
- [18] D Y Shang, X P Li, M Yin, et al. Rotation angle control strategy for telescopic flexible manipulator based on a combination of fuzzy adjustment and rbf neural network. *Chinese Journal of Mechanical Engineering*, 2022, 35: 53.
- [19] S S Han, H P Wang, Y Tian, et al. Time-delay estimation based computed torque control with robust adaptive rbf neural network compensator for a rehabilitation exoskeleton. *ISA Transactions*, 2020, 97: 171-181.
- [20] Y Wang, W Zhang, D Shi, et al. Design and control of an adaptive knee joint exoskeleton mechanism with buffering function. *Sensors (Basel)*, 2021, 21(24): 8390.
- [21] Z L Chen, Q Guo, H Y Xiong, et al. Control and implementation of 2-dof lower limb exoskeleton experiment platform. *Chinese Journal of Mechanical Engineering*, 2021, 34:22.
- [22] Z L Chen, Q Guo, T S Li, et al. Output constrained control of lower limb exoskeleton based on knee motion probabilistic model with finite-time extended state observer. *IEEE-ASME Transactions on Mechatronics*, 2023.
- [23] Y Long, Y J Peng. Extended state observer-based nonlinear terminal sliding mode control with feedforward compensation for lower extremity exoskeleton. *IEEE Access*, 2022, 10: 8643-8652.
- [24] X S Gao, P F Zhang, X F Peng, et al. Autonomous motion and control of lower limb exoskeleton rehabilitation robot. *Frontiers in Bioengineering and Biotechnology*, 2023, 11.
- [25] J Y Song, A B Zhu, Y Tu, et al. Novel design and control of a crank-slider series elastic actuated knee exoskeleton for compliant human-robot interaction. *IEEE-ASME Transactions on Mechatronics*, 2023, 28(1): 531-542.
- [26] I Poultagari, R Shahnazi, M Sheikhan. Rbf neural network based pi pitch controller for a class of 5-mw wind turbines using particle swarm optimization algorithm. *ISA Transactions*, 2012, 51(5): 641-648.
- [27] B Ren, X R Luo, Y Wang, et al. A gait trajectory control scheme through successive approximation based on radial basis function neural networks for the lower limb exoskeleton robot. *Journal of Computing and Information Science in Engineering*, 2020, 20(3).
- [28] M K Duong, H Cheng, H T Tran, et al. Minimizing human-exoskeleton interaction force using compensation for dynamic uncertainty error with adaptive rbf network. *Journal of Intelligent & Robotic Systems*, 2016, 82(3-4): 413-433.
- [29] Y Chen, J Y Liu, H P Wang, et al. Model-free based adaptive rbf neural network control for a rehabilitation exoskeleton. *31st Chinese Control And Decision Conference (CCDC)*, Nanchang, China, 2019.
- [30] Y Yang, X C Dong, Z Q Wu, et al. Disturbance-observer-based neural sliding mode repetitive learning control of hydraulic rehabilitation exoskeleton knee joint with input saturation. *International Journal of Control Automation and Systems*, 2022, 20(12): 4026-4036.
- [31] C L Vaughan, B L Davis, J O'Connor. Dynamics of human gait. 1999.
- [32] F Sado, H J Yap, R A R Ghazilla, et al. Design and control of a wearable lower-body exoskeleton for squatting and walking assistance in manual handling works. *Mechatronics*, 2019, 63: 102272.
- [33] C Wang, D J Hill. Learning from neural control. *IEEE Transactions on Neural Networks*, 2006, 17(1): 130-146.
- [34] Y P Pan, T R Sun, Y Q Liu, et al. Composite learning from adaptive back-stepping neural network control. *Neural Networks*, 2017, 95: 134-142.

[35] E Reznick, K R Embry, R Neuman, et al. Lower-limb kinematics and kinetics during continuously varying human locomotion. *Scientific Data*, 2021, 8(1): 282.

Yibo Han born in 1997, is currently a PhD candidate at *Robotics Institute, Beihang University, China*. He received his bachelor degree from *Shandong University, China*, in 2019. And he received his master degree from *Beihang University, China*, in 2022. His research interests include wearable robotics.

Hongtao Ma is currently the senior software director of *Beihang Goer (WeiFang) Intelligent Robot Co., Ltd., China*. He received bachelor degree in computer and its application from *Shandong University, China*, in 1988. His research interests include industrial automation and distributed real-time embedded system.

Yapeng Wang is currently a PhD candidate at *Research Center of Satellite Technology, Harbin Institute of Technology, China*. His research interests include wearable robotics.

Di Shi is currently a Postdoctoral Researcher at *Robotics Institute, Beihang University, China*. He received his PhD degree from *Beihang University, China*, in 2021. His research interests include wearable lower limb rehabilitation robot control.

Yanggang Feng is currently an assistant professor at *School of Mechanical Engineering and Automation, Beihang University, China*. He received his PhD degree from *Peking University, China*, in 2019. His research interests include wearable robotics and AI.

Xianzhong Li is currently a PhD candidate at *Robotics Institute, Beihang University, China*. His research interests include wearable robotics.

Yanjun Shi is currently a master candidate at *Robotics Institute, Beihang University, China*. His research interests include wearable robotics.

Xilun Ding is currently a professor and a PhD candidate supervisor at *School of Mechanical Engineering and Automation, Beihang University, China*. He received his PhD degree from *Harbin Institute of Technology, China*, in 1997. His research interests include the dynamics of compliant mechanical systems and robots, nonholonomic control of space robots, dynamics and control of aerial robots, and biomimetic robots.

Wuxiang Zhang is currently a professor at *School of Mechanical Engineering and Automation, Beihang University, China*. He received his PhD degree from *Beihang University, China*, in 2009. His research interests include the dynamics of compliant mechanical systems and robots, intelligent device and detection technology.